MICROSTRUCTURAL CHARACTERIZATION OF LPCVD TUNGSTEN INTERFACES

D.C. PAINE*, J.C. BRAVMAN*, AND K.C. SARASWAT**
*Stanford University, Dept. of Materials Science, Bldg. 550, Stanford, CA 94305
**Stanford University, Center for Integrated Systems, Stanford, CA 94305

ABSTRACT

From a materials viewpoint many process-dependent characteristics of LPCVD tungsten have yet to be detailed. Specifically, there exists at the tungsten/silicon interface a number of morphological features which occur on a submicron to atomic level. These include lateral encroachment of tungsten beneath silicon/silicon dioxide interfaces, the formation of "wormholes" in the silicon substrate, and tungsten/silicon interfacial roughness. In this work, cross-section TEM is used to characterize the above morphologies. Evidence for the mechanism of formation for several of these morphologies is presented.

INTRODUCTION

Many of the developmental challenges which must be overcome before low pressure chemical vapor deposition (LPCVD) of tungsten can be implemented on a commercial scale involve control of morphological features which occur on submicron-to-atomic levels. Problems of this sort are particularly well suited for study by cross-sectional transmission electron microscopy (XTEM). In an earlier work [1], several such features were identified using XTEM. Problems include lateral encroachment of tungsten beneath silicon-silicon dioxide interfaces, the formation of so called wormholes or filamental tunnels in the silicon substrate, and tungsten-silicon interfacial roughness. All of these features have potentially adverse effects on device reliability, device performance, and the ability to fabricate reproducable ohmic contacts. For this reason, an analysis and complete understanding of the mechanisms involved in the formation of these submicron to atomic scale features is required.

The use of XTEM to resolve interface roughness, microstructure, and second phase particles is well established. A particularly important area where XTEM has proven its worth is in the investigation of interfaces in electronic materials. For determining structure and morphology at interfaces, XTEM is superior to the surface averaging techniques such as Auger, XPS, and RBS. In these techniques, depth resolution is, at best, on the order of 0.5 to 1 nm. Resolution on this scale, however, is lost unless the interface region being analysed is planar. This is because surface averaging techniques have a lateral resolution which is limited to one or more microns. When the interface is rough on a scale that is less then the lateral resolution of the technique being used, averaging occurs which eliminates the advantages of the good depth resolution. Similarly, surface averaging techniques are poorly suited for the identification of microprecipitates of a second phase material. The problem becomes even worse when the second phase material is composed of the same elements which make up the interfacial region. A small amount of tungsten silicide at the interface between tungsten and silicon is an example of a second phase which would be difficult or impossible to detect using these techniques.

The chemistry of LPCVD tungsten using WF_6 has been detailed elsewhere [2]. A review of the principal elements, however, follows. When WF_6 is initially introduced into a furnace loaded with silicon wafers, contact with the exposed silicon above 300°C will lead to the reaction:

$$2WF_6 + 3Si = 3SiF_4 + 2W$$

The reduction of the WF_6 continues until the deposited tungsten layer becomes thick enough (usually about 10 nm) to seal the silicon surface, thus preventing any further reduction by silicon. In order to produce thicker tungsten deposits, hydrogen gas is introduced into the reactor to reduce the WF_6 via the reaction:

$$WF_6 + 3H_2 = W + 6HF$$

2nd Workshop on Tungsten Albuquerque, Oct. 1985 (INVITED)

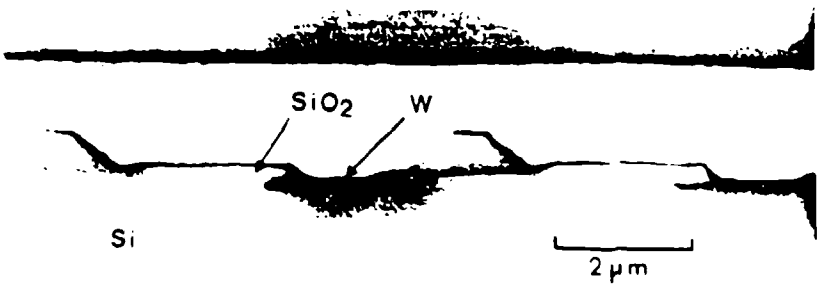

Fig. 1. Non-selective tungsten on patterned silicon.

The ultimate thickness of the tungsten film produced by the initial reaction is reached in a few seconds, and is fairly independent of temperature. The ultimate thickness produced by the hydrogen reaction, however, is linear with time, and has a square-root dependence on the hydrogen partial pressure. This indicates [2] that the dissociation of hydrogen on tungsten is the rate limiting step. Thus, tungsten deposited by the initial silicon reaction catalyzes further deposition by the hydrogen reaction. It is this characteristic that makes LPCVD tungsten a selective process. Since clean, untreated silicon dioxide can neither reduce WF_6 nor provide nucleation sites for hydrogen reduction, tungsten is deposited selectively on exposed silicon. It is clear that the physical properties of the initial 10 nm of tungsten will play a role in interface morphology development.

EXPERIMENTAL

In order to effectively study selectively deposited tungsten using XTEM, a TEM-dedicated test structure was used. This structure consists of repeating parallel lines of selective tungsten evenly spaced with 2 μm wide lines of 100 nm thick silicon dioxide then 2 μm wide lines of 500nm oxide. The processing was as follows. First a field oxide approximately 500nm thick was grown using standard dry-wet-dry oxidation at 1000 °C. The dry cycles of the oxidation were 10 minutes long while the intermediate wet oxidation was for 150 minutes. The field oxide was patterned by etching 4 μm wide and 9 mm long implant windows. Next, a dose of $2x10^{16}/cm^2$ arsenic was implanted at 100KeV. A thinner, 100nm oxide was then grown over the implanted region as part of an oxidation, anneal, and drive-in step. Once again a dry-wet-dry oxidation at 950 °C was done with 10 minute dry cycles and a 20 minute wet cycle. Contact holes 2 μm wide were then plasma etched into the thin oxide. A standard RCA clean was performed prior to tungsten deposition. A cross-sectional TEM micrograph showing the line structure is seen in Figure 1. In Figure 1 tungsten can be seen on both exposed silicon and on the oxide. This was a result of reactor contamination. After the reactor was cleaned, samples showed complete selectivity. In addition to the patterned wafers, blanket depositions of tungsten on bare silicon wafers were also produced. All of the tungsten depositions were done in a 3 inch hot wall LPCVD reactor. The total pressure in the reactor was maintained at 0.25 torr. The deposition temperature was 300 °C. Gas flows were: WF_6, 10 cc/min., and H_2, 75 cc/min. This produced a deposition rate of 3.5 nm per minute. Finally, XTEM samples were fabricated using standard [3] techniques.

RESULTS

Lateral Encroachment

In the worst of the observed cases, lateral encroachment was seen to extend up to 0.7μm under the thin oxide from a 2 μm contact hole. Associated with this extensive encroachment was the presence of implanted arsenic. Figure 1 shows that encroachment has occured only under the implanted region beneath the thin oxide. The region under the thick oxide, used as an implant mask, shows no lateral encroachment.

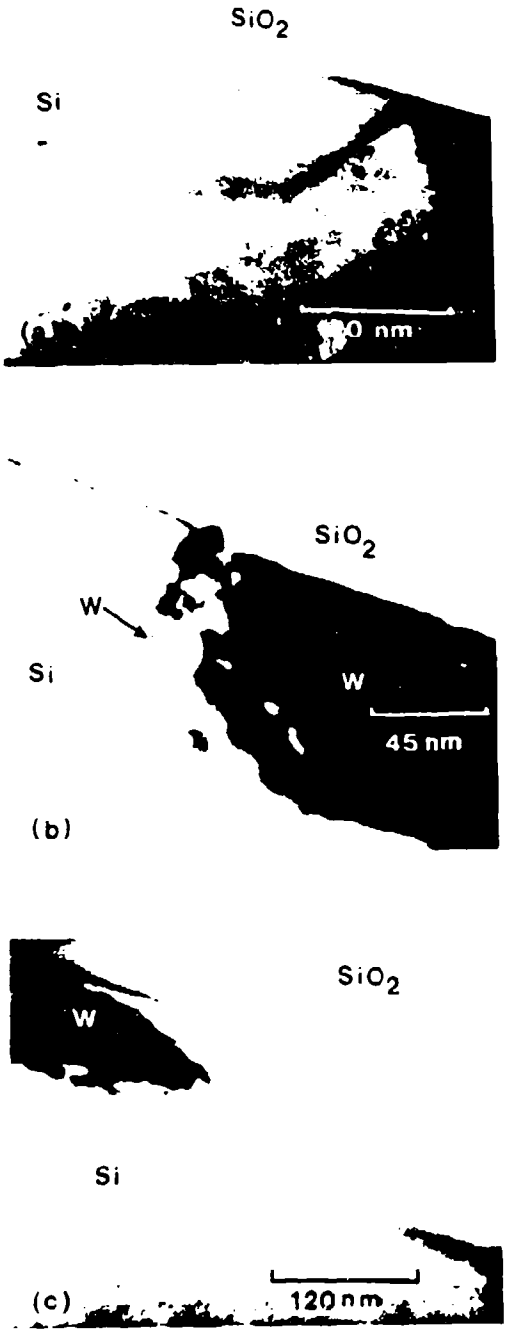

Fig. 2. (a) Dislocations in implanted region of silicon below thin oxide.
(b) Lateral encroachment of tungsten beneath thin silicon oxide. Dislocation immediately ahead of encroachment front shows tungsten deposits.
(c) Encroachment following a dislocation which runs out of the plane of the picture. A dislocation loop is also visible.

Evidence implicating residual implant damage as a cause for the extensive lateral encroachment observed is shown in Figures 2(a), (b), and (c). These micrographs were taken in the region just ahead of the 0.7μm encroachment front. In Figure 2(a) a dislocation loop under the thin oxide is shown. In this case, the dislocation is pinned at one end by the oxide/silicon interface and, at the other end, by another dislocation running approximately perpendicular to the plane of the micrograph. Subsequent high resolution microscopy was used to establish that these defects are dislocations rather than stacking faults or microtwins which are more commonly found in silicon.

Figure 2(b) shows the encroachment front. Immediately ahead of the front is a dislocation which has been decorated with large tungsten precipitates. This provides solid evidence that residual ion implant damage has played an important role in enhancing the motion of the encroachment front. In Figure 2(c), a different encroachment morphology is seen. In this case, the encroachment has followed a dislocation which runs parallel to the oxide/silicon interface. The presence of this dislocation has lead to tungsten extending through the silicon without disturbing the silicon immediately under the silicon/silicon dioxide interface.

In the best of the observed cases, encroachment extended only 0.2 μm under the thin oxide. Associated with this reduced encroachment was a reduction in the number of defects seen under the thin oxide. In many of these samples, wormhole structures could be seen extending out in front of the 0.2 μm encroachment front as shown in Figure 3. These tunnels are relatively short (150nm) and may play a role in the development of lateral encroachment in the absence of dislocations. The wormhole mechanism will be discussed in detail later. Their presence, however, in the 0.2 μm case and not in the 0.7 μm case may simply be due to the lateral encroachment progressing to the point where the tunnels were over-run in the latter but not in the former.

Interface Roughness

The tungsten/silicon interface region is seen in Figure 4. While most of the tungsten overlayer has been milled away during TEM specimen preparation, the remaining tungsten shows an interface roughness of approximately 20nm. The origin of interface roughness appears to be due to two mechanisms. For large scale roughness, native oxide patches can be seen to be present at the interface. The presence of oxide protects the underlying silicon during the silicon reduction stage of the deposition of tungsten from WF_6. Consequently, only those regions exposed to the WF_6 will be consumed during the

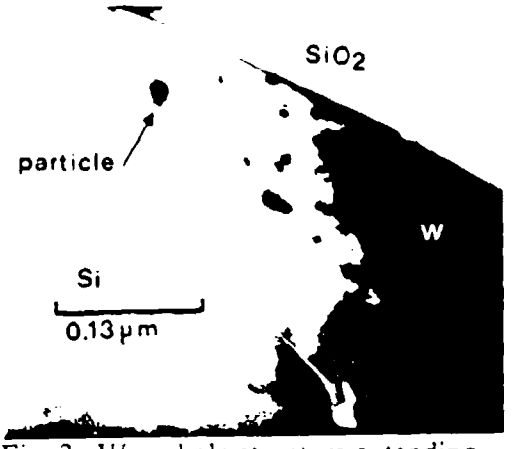

Fig. 3. Wormhole structure extending in front of a 0.2 µm encroachment front.

initial silicon reduction stage. This is in agreement with others [1] who showed that surface preparation plays an important role in determining interfacial morphology.

A proposed second mechanism for interface roughness is the formation of silicide protrusions in isolated regions of the tungsten silicon interface. It is well known from thermochemical data that tungsten silicide is thermodynamically stable at 300°C. In general, however, silicide formation at these low temperatures is not kinetically feasible due to decreased atomic mobility. Two separate TEM experiments, however, have provided evidence for the the presence of very small amounts of a silicide phase at the tungsten/silicon interface. Figure 5 shows a high resolution image of a protrusion originating in the tungsten layer and projecting into the silicon. The protrusion shows light and dark bands known as Moire fringes running approximately across the width of the protrusion. Moire fringes result from the interaction of two overlaid diffracting crystals which are misoriented with respect to each other and/or have different interplanar spacings. The planes that form the Moire pattern must lie in the zone defined by the incident electron beam. In Figure 5, one of the crystals involved in the formation of the Moire pattern is the silicon substrate which is oriented in the [110] zone. The possible plannar spacings of the second, unknown, crystal can be readily determined by the relationship $g=g_1-g_2$, where g_1 is the silicon reciprocal lattice vector and g_2 is the reciprocal lattice vector of the plane in the unknown crystal. The orientation and fringe spacing from the Moire pattern defines g. All the possible g_1 vectors for silicon oriented in the [110] zone and g of the moire pattern is known, hence, it is easy to determine the various g_2 vectors which are consistent with g_1 and g. An optical bench is used to obtain a high degee of acuracy for g_1 and g. The analysis, even with a generous allowance for measurement error, shows that there are no low index planes in either tungsten or silicon which could have caused these Moire fringes Higher index silicon reflections such as 331 could, in principle,interact with tungsten to cause these fringes. These higher order reflections,however, were dismissed because diffraction patterns from the silicon in the region of interest showed that the higher order reflections are of low intensity. The Moire pattern shown in Figure 5 is very well defined. This indicates that it was formed from strongly diffracting planes (i.e. low index planes) in both crystals. This seems to suggest that the protrusion is not tungsten but rather one of the tungsten silicides, all of which have low index planes which would fit this data.

With this knowledge, preliminary electron diffraction data was obtained in an effort to establish the identity of the unknown phase. A series of diffraction patterns as close as possible to the interfacial region were taken using a 20nm electron probe. A resulting diffraction pattern is seen in Figure 6. Near the silicon/tungsten interface the tungsten grain size becomes very small. Due to the very small grain size of both the tungsten (<20nm) and the second phase, several

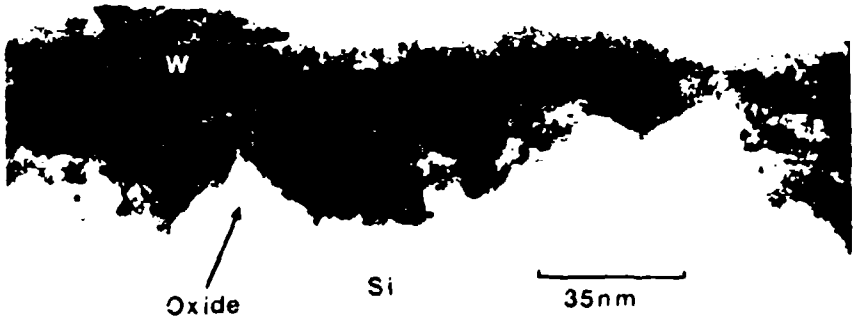

Fig. 4. Tungsten/silicon interface region. Most of the tungsten has been milled away during sample preparation.

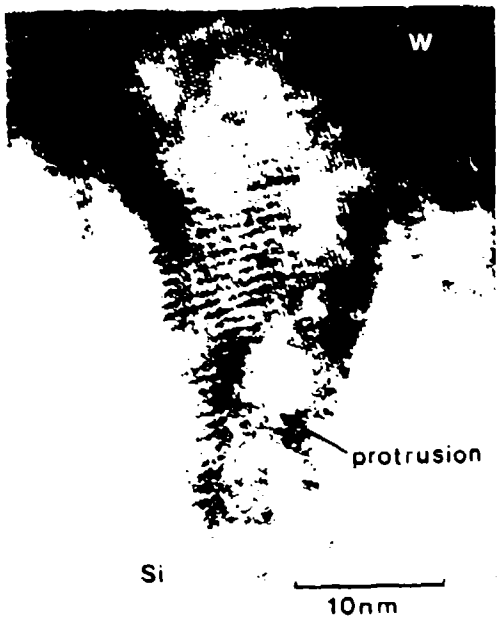

Fig. 5. Protrusion into the silicon substrate originating in the tungsten overlayer. Moire fringes are clearly visible as light and dark bands running part way across the width of the protrusion.

grains are included by the 20nm probe and hence we see several overlapping patterns. The points labeled are consistent with a tungsten grain oriented near the <153> zone. Additional points are associated with a different tungsten grain oriented near the <321> zone. Some of the faint reflections can be shown to be due to double diffraction phenomena. The pairs of reflections labeled D and G are from a crystal with interplanar spacings of 0.213+/-0.008 nm and 0.247+/-0.01nm respectively.

These interplanar distances are not present in either tungsten or silicon. Both the hexagonal phase of tungsten disilicide, and the tetragonal W_5Si_3 phase, have d spacings which match those seen above within the measurement error. The D reflection has a spacing which is close to the hexagonal {111} plane (0.2166 nm), as well as the {003} plane (0.2132 nm). The tetragonal phase {421} plane (0.214 nm) is also a possibility. The G reflection is consistent with the hexagonal {102} plane (0.2498 nm) and the tetragonal {002} plane (0.248 nm). Neither phase, however, can be identified from this diffraction pattern since the angular relationship between the two reflections, D and G, does not closely fit the hexagonal silicide and, though the angular relationship is close, the d spacing is just outside the expected error for the tetragonal {321} and {022} reflections. The angle measured between the reflections D and G is 51 degrees. The multiplicity of equivilent planes in the hexagonal system is twelve making the number of different interplanar angles large. All of these angles were checked. The lack of angular agreement in the either case may be due to the unknown crystal being twinned or due to the presence of two of the unknown crystals diffracting. Another possibility is that an unknown metastable silicide is present.

The idea that microprecipitates of silicide should be present at these low temperatures is not unreasonable. Using X-ray diffraction, the hexagonal tungsten silicide phase has been seen [4] at temperatures as low as 550 °C. The minimum amount of silicide necessary to give a detectable X-ray signal would be many times greater then the amount observed at the tungsten/silicon interface in this work. Other workers [5] have observed up to ten monolayers of tungsten silicide formed at room temperature when silicon is evaporated onto tungsten.

Stress measurements in an as-deposited blanket tungsten film have suggested a possible mechanism for silicide formation which will explain the presence of a silicide phase at these low (300 °C) temperatures. The residual stress in one of the blanket tungsten deposits was measured using an optical lever technique. This technique, first described [6] in 1978, reliably measures stress levels in thin films with an accuracy of approximately 10 MPa. The results obtained from our blanket tungsten show a residual stress level of 1.1 GPa. At first this seems surprisingly high; equally thick evaporation deposited films of aluminium measured on the same apparatus show residual tensile stress levels of 100-300 MPa. The thermal expansion coefficient of aluminium (23.6ppm/°C) is many times greater than that for tungsten (4.5ppm/°C) or silicon (3.0ppm/°C). This illustrates that although it is true that tungsten has a thermal expansion coefficient closest to that of silicon, it is not this parameter

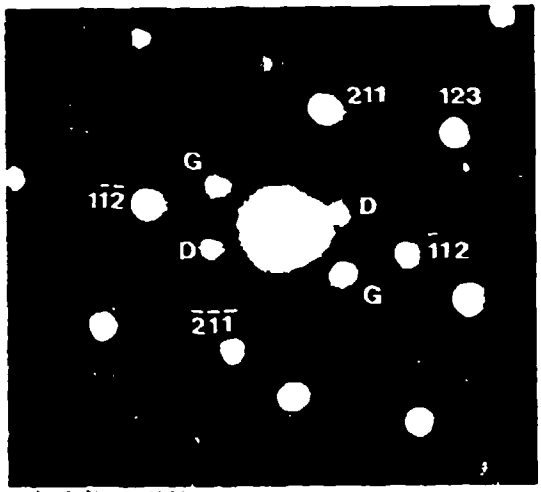

Fig. 6. Microdiffraction pattern from near the tungsten/silicon interface.

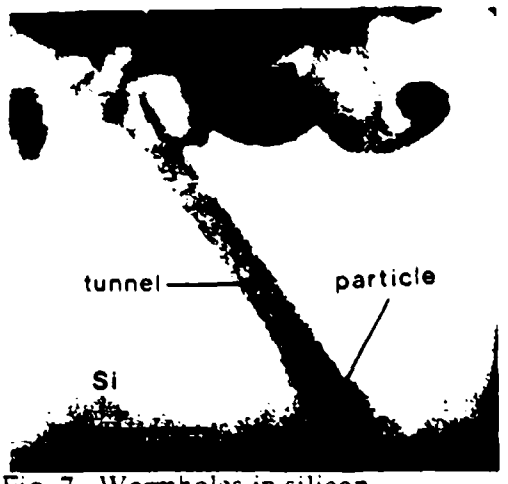

Fig. 7. Wormholes in silicon.

alone which determines residual stress in a thin film. One must also consider (among other things) the much higher yield strength of tungsten compared to aluminium. Since tungsten has a very high yield strength (made even higher by its 20–100 nm grain size), it can support higher stress levels. One mode whereby this stress could be relieved is by the formation of silicide. The high tensile stress levels, either as the wafer is cooled to room temperature or as a result of intrinsic stresses due to the deposition process, can be relieved by the expansion which is attendent to silicide formation. This stress relief provides a significant additional driving force for silicide formation.

Wormholes

The presence of filamental tunnels in LPCVD tungsten on silicon has been noted by several workers. In the current work, short (<100nm) wormhole structures have been observed under blanket deposited tungsten and, in some circumstances, in advance of the lateral encroachment front. Much longer tunnels are seen, when implant damage is absent, in the corner region where silicon dioxide, silicon, and tungsten meet. The ubiquitous nature of the tunnel structures seems to indicate that their presence is a consequence of the tungsten/silicon interface chemistry.

Observations of wormholes which have already appeared in the literature [1] and which are in agreement with the present work are as follows. (1) The wormholes consist of empty tunnels in silicon which can be up to 1 micron long and are typically 20-40 nm wide. (2) A tungsten-rich particle is always found at the end of the each tunnel. (3) The path the tunnel takes appears to be random. (4) The particle is neither consumed nor enlarged during the tunneling reaction. Figure 7 shows a typical wormhole structure in which one particle moves in a straight path while another travels in a helical path. High resolution TEM allows us to lattice image the silicon in the region around the tunnel structure as shown in Figure 8. Other lattice resolution images (not shown) of the tunnel region shows that there is no crystallography associated with the path of the particle through the silicon.

The evidence for the presence of silicide at the tungsten/silicon interface leads to the proposal of the following mechanism for the formation of the wormhole structure.

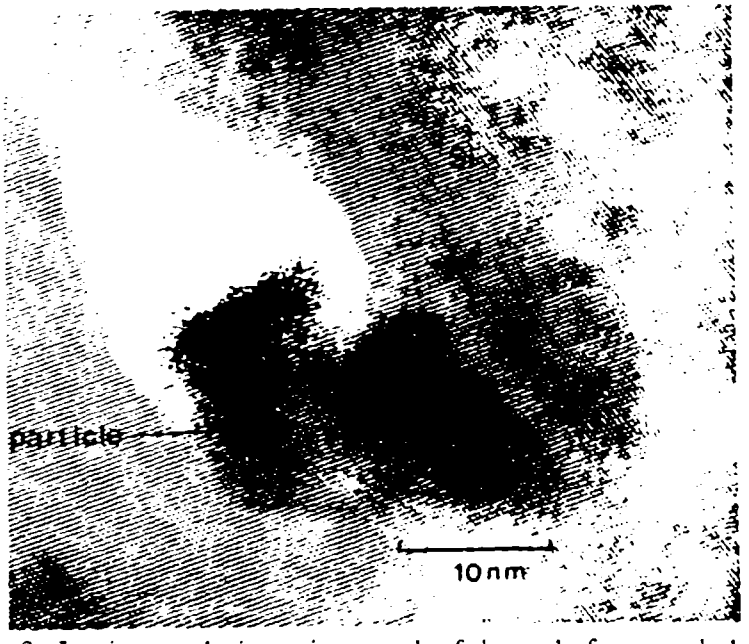

Fig. 8. Lattice resolution micrograph of the end of a wormhole.

This mechanism predicts the presence of a tungsten silicide particle rather than an elemental tungsten particle at the end of the tunnel. This has not yet been uniquely established because of the experimental difficulties associated with obtaining an electron diffraction pattern from such a small (≅20nm) second phase particle embedded in a thicker, strongly diffracting matrix. In addition, the widely different ion milling rates of tungsten, silicon, and silicon oxide makes isolation of a wormhole particle a rare event. The suggestion of a silicide, however, based on earlier arguments, does not seem unreasonable. Since elemental tungsten is a diffusion barrier to

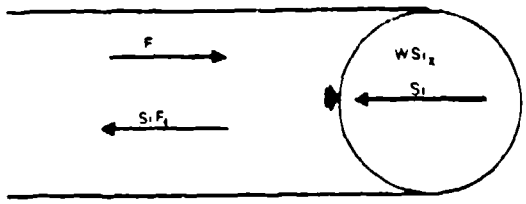

Fig. 9. Schematic representation of the proposed wormhole mechanism.

silicon even at 300 °C, the presence of a silicide explains how rapid diffusion of silicon through the particle can occur. Silicon diffusion through silicide is rapid, thus either molecular flourine or HF, present due to the reduction of WF_6, can react with silicon in the particle at its trailing edge. This causes a concentration gradient between the silicon-depleted trailing edge and the silicon-rich silicon/silicide interface. Gas transport of SiF_4 gas back out of the tunnel completes the removal of silicon. The mechanism is shown schematically in Figure 9.

The proposed mechanism is analagous to the oxidation of silicide on silicon. In this case, silicon is consumed as it diffuses through the silicide layer from the silicon bulk, forming silicon dioxide on the silicide surface. The silicide is neither consumed nor enlarged by the oxidation but simply moves down through the silicon as an oxide layer builds up on its surface. Morphological features similar in many respects to the wormholes in tungsten/silicon have recently been seen in the oxidation of titanium silicide [7]. When titanium silicide on silicon is oxidized, nodules of silicide detach from the bulk and begin tunneling through the silicon. The details of the mechanism of formation of these tunnels is not clear. It should be noted, however, that the tunnels are much shorter (50 nm) then in the LPCVD tungsten case.

SUMMARY

Three important interfacial morphologies are observed in LPCVD tungsten on silicon: lateral encroachment, interface roughness, and wormhole structures. They have been shown to be, in part at least, a result of defect condition. Defects which have been positively identified using XTEM include residual native oxide and dislocations from ion implantation. A third phase, possibly tungsten silicide, has been observed but not uniquely identified.

Extensive lateral encroachment has been shown to be related to the presence of residual implant damage. Specifically, dislocation loops under oxide grown over arsenic implanted silicon were implicated. Interface roughness appears to result from both residual native oxide patches on the silicon surface as well as to the formation of small protrusions of a third, probably silicide phase. The electron microscopy techniques of microdiffraction and Moire analysis were used in an attempt to identify the third phase. The presence of a third phase has lead to the proposal of a mechanism for the formation of the wormhole structure. Additional work, currently underway, will establish the identity of both the interfacial phase and the wormhole particles.

The assistance of P. Townsend in providing stress measurements, and T. Schreyer, B. Loh, and H. Wulu in providing tungsten samples, is gratefully acknowledged.

REFERENCES

(1) W.T. Stacy, E.K. Broadbent, and M.H. Norcott, J. Electrochem. Soc., 132, 444 (1985)

(2) E.K. Broadbent and C.L. Ramiller, J. Electrochem. Soc., 131, 1427 (1984)

(3) J.C. Bravman, and R. Sinclair, J. Electron. Micros. Tech., 1, 53 (1984)

(4) F.M. d'Heurle, C.S.Petersson, and M.Y. Tsai, J. Appl. Phys., 51, 5976 (1981)

(5) S. Weng, Phys. Rev. B, 29, 2363 (1984)

(6) A.K. Sinha, H.J. Levinstein, and T.E. Smith, J. Appl. Phys., 49, 2423 (1978)

(7) R. Beyers, to be published

END

DTIC

7-86